AIP Journal of Applied Physics

Poole-Frenkel-effect as dominating current mechanism in thin oxide films—An illusion?!

Herbert Schroeder

Citation: Journal of Applied Physics **117**, 215103 (2015); doi: 10.1063/1.4921949
View online: http://dx.doi.org/10.1063/1.4921949
View Table of Contents: http://scitation.aip.org/content/aip/journal/jap/117/21?ver=pdfcov
Published by the AIP Publishing

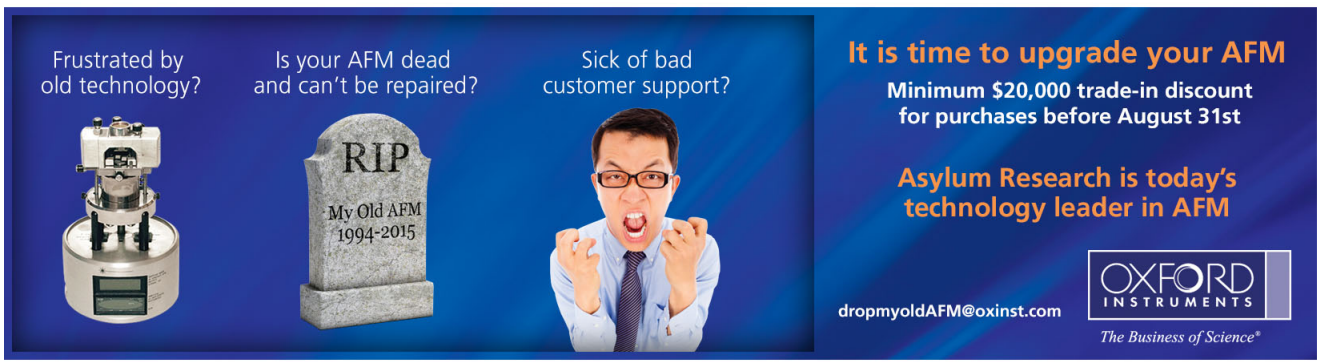

Poole-Frenkel-effect as dominating current mechanism in thin oxide films—An illusion?!

Herbert Schroeder
Electronic Materials, PGI-7, Research Center Jülich, 52425 Jülich, Germany

(Received 30 December 2014; accepted 20 May 2015; published online 5 June 2015)

In many of the publications, over 50 per year for the last five years, the Poole-Frenkel-effect (PFE) is identified or suggested as dominating current mechanism to explain measured current–electric field dependencies in metal-insulator-metal (MIM) thin film stacks. Very often, the insulating thin film is a metal oxide as this class of materials has many important applications, especially in information technology. In the overwhelming majority of the papers, the identification of the PFE as dominating current mechanism is made by the slope of the current–electric field curve in the so-called Poole-Frenkel plot, i.e., logarithm of current density, j, divided by the applied electric field, F, versus the square root of that field. This plot is suggested by the simplest current equation for the PFE, which comprises this proportionality ($\ln(j/F)$ vs. $F^{1/2}$) leading to a straight line in this plot. Only one other parameter (except natural constants) may influence this slope: the optical dielectric constant of the insulating film. In order to identify the importance of the PFE simulation studies of the current through MIM stacks with thin insulating films were performed and the current–electric field curves without and with implementation of the PFE were compared. For the simulation, an advanced current model has been used combining electronic carrier injection/ejection currents at the interfaces, described by thermionic emission, with the carrier transport in the dielectric, described by drift and diffusion of electrons and holes in a wide band gap semiconductor. Besides the applied electric field (or voltage), many other important parameters have been varied: the density of the traps (with donor- and acceptor-like behavior); the zero-field energy level of the traps within the energy gap, this energy level is changed by the PFE (also called internal Schottky effect); the thickness of the dielectric film; the permittivity of the dielectric film simulating different oxide materials; the barriers for electrons and holes at the interfaces simulating different electrode materials; the temperature. The main results and conclusions are: (1) For a single type of trap present only (donor-like or acceptor-like), none of the simulated current density curves shows the expected behavior of the PFE and in most cases within the tested parameter field the effect of PFE is negligibly small. (2) For both types of traps present (compensation) only in the case of *exact* compensation, the expected slope in the PF-plot was nearly found for a wider range of the applied electric field, but for a very small range of the tested parameter field because of the very restricting additional conditions: first, the quasi-fermi level of the current controlling particle (electrons or holes) has to be 0.1 to 0.5 eV closer to the respective band limit than the zero-field energy level of the respective traps and, second, the compensating trap energy level has to be shallow. The conclusion from all these results is: the observation of the PFE as dominating current mechanism in MIM stacks with thin dielectric (oxide) films (typically 30 nm) is rather improbable! © *2015 AIP Publishing LLC*.
[http://dx.doi.org/10.1063/1.4921949]

INTRODUCTION

In solid state and materials engineering textbooks, one can find in the sections about "Conduction" or "(Leakage) Current" through metal-insulator (wide band gap semiconductor)-metal (MIM) stacks usually two classes in models for the (leakage) current:

(a) Current is interface controlled, e.g., thermionic (field) emission; tunneling carrier injection.
(b) Current is bulk controlled, e.g., space charge limited current (SCLC); Poole-Frenkel-effect (PFE).

Therefore, it is not surprising that in the literature this classification of the suggested current mechanisms into these classes is applied nearly without exception. But even in the simplest versions of these models, many assumptions and restrictions have to be fulfilled in order that one of these mechanisms is really controlling the leakage current in MIM stacks. In the literature, very often these conditions are not mentioned or observed when such mechanisms are suggested to describe experimental leakage results. Moreover, the classification into (a) and (b) is anyway very crude, as in any MIM at least one mechanism of each class is working at the same current level in order to describe the steady-state leakage current so that a better description would be by models combining at least one mechanism of each class consistently. This is even more important for thin films for which the interface regions usually occupy larger portions of the film

thickness, so that undisturbed bulk properties cannot be assumed for most of the film thickness anymore, i.e., an essential condition leading to bulk controlled mechanisms.

For all these reasons, a combined model was developed using thermionic field emission for carrier injection (and ejection) (Schottky effect (SE)) at the interfaces and drift-diffusion current in the bulk consistently bound together at the two MI interfaces by a condition suggested by Crowell, Beguwala, and Sze.[1,2] This model has been described in detail in papers before[3–5] and will be outlined shortly in a section below.

In the literature, over 50 papers per year are listed in abstract search programs if you enter "Poole-Frenkel" AND "thin films" AND "mechanism OR model" as search topics, presuming that in most of these papers the PFE is suggested as dominating, bulk-controlled leakage current mechanism, as sample inspections of these papers have approved.[6] And nearly always the most simple PFE current equation[7–9] was used to fit experimental data, i.e., a straight line in the "PF-plot," which is log(current density j/applied electric field F) vs. (applied electric field F)$^{1/2}$.

For the reasons mentioned above, the combined simulation tool was used to test if an implementation of the PFE would change the simulated current curves and under which parameter sets the changes occur, and if the changed curves represent the characteristic dependencies for the PFE. The aim of the reported investigations is to define these parameter sets with respect to interface properties such as injection/ejection barrier height, to film properties such as thickness and permittivity, and to trap properties, which are the reason for the appearance of the PFE, such as type, density, and energy level in the gap.

The reported results suggest that the implementation of the PFE does not change the leakage current in most cases of the tested parameter field. For the few changed cases, many of them do not show the expected characteristic slope in the PF-plot. Only in a rather small range of the tested parameter field, the simulation data show nearly the expected PFE behavior so that PFE may be identified under these conditions as dominating mechanism for the (leakage) current through MIM thin film stacks over a significant range of the applied electric field and temperature. But as these conditions are quite stringent and to some extent not realistic, the appearance of the PFE as controlling current mechanism in thin film MIM stacks is rather improbable, in contrast to its numerous citations in the literature.

THE POOLE-FRENKEL EFFECT (PFE)

The PFE is applicable if the trap center is *neutral* with the captured carrier (e^-, h^+), as only then an attractive (coulomb) interaction is working when the charged carrier escapes from the then charged trap! The general mechanism of the PFE is sketched in Fig. 1: The barrier $e_0\Phi_{tn} = |E_C - E_{tn}|$ for an electron to escape from its trap at energy level E_{tn} into the conduction band (and a barrier $e_0\Phi_{tp} = |E_{tp} - E_V|$ for a hole to escape into the valence band, respectively) is equal in both directions in this simplified linear model for the field-free state ($F = 0$). This is changed

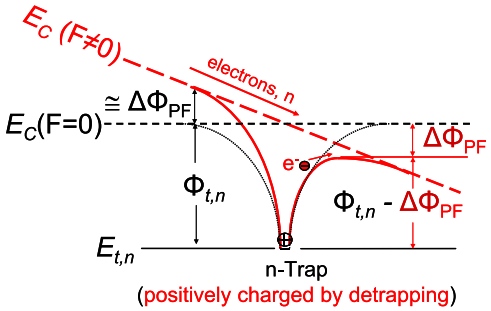

FIG. 1. Schematic sketch of the Poole-Frenkel-effect without and with electric field, F.

by the presence of an electric field $F \neq 0$: In forward direction (in our case, the direction of the drift of the electrons), the barrier is diminished by $\Delta\Phi_{PF}$ compared to the field free state by the applied and/or internal electric field F with appropriate sign. A field with the opposite sign enlarges the barrier in the same direction by about the same value. Usually, the coulomb interaction between the leaving carrier and remaining charged trap is used. Therefore, the barrier reduction $\Delta\Phi_{PF}$ is similar to that for the SE in the thermionic emission with an electric field present. The difference is that the trap is localized (spatially fixed) while in the Schottky emission both interacting charges are moving: This results in a barrier reduction $\Delta\Phi_{PF}$ twice as large as in the Schottky effect, $\Delta\Phi_{SE}$.

$$e_0\Delta\Phi_{PF} = [(e_0^3F)/(\pi\,\varepsilon_{r,\,opt}\varepsilon_0)]^{1/2} = 2e_0\Delta\Phi_{SE}\ [\mathrm{eV}], \qquad (1)$$

with e_0 the elementary charge, ε_0 the vacuum permittivity, and $\varepsilon_{r,opt}$ the relative optical (high frequency) permittivity (relative optical dielectric constant) of the insulating film material.

With the reduced barrier, the escape from the trap happens more often and, therefore, the corresponding densities of free carriers in the bands, n_{PF} (electrons) or p_{PF} (holes), are higher in the average than without the implementation of PFE, possibly increasing the (leakage) current due to the increased PF-conductivity $\sigma_{PF} = e_0\mu_n n_{PF}$ (for electrons) compared to the *low field* conductivity $\sigma_0 = e_0\mu_n n_0$ (or *without* PFE implementation):

$$\sigma_{PF} = e_0\mu_n n_{PF} = e_0\mu_n n_0 \exp\left\{\frac{e_0\Delta\Phi_{PF}}{k_BT}\right\}$$
$$= e_0\mu_n n_0 \exp\left\{\frac{e_0}{k_BT}\left(\frac{e_0}{\pi\,\varepsilon_{r,\,opt}\varepsilon_0}\right)^{1/2}F^{1/2}\right\}, \qquad (2)$$

with μ_n the field independent electron mobility, k_B the Boltzmann constant, and T the temperature.

This results in the often cited PF current density[9]

$$j_{PF} \propto F\exp\left\{-\frac{e_0}{k_BT}\left[\Phi_t - \left(\frac{e_0}{\pi\,\varepsilon_{r,\,opt}\varepsilon_0}\right)^{1/2}F^{1/2}\right]\right\}. \qquad (3a)$$

Using the characteristic PF-plot, i.e., $\ln(j_{PF}/F)$ vs. $F^{1/2}$, a straight line should fit the leakage current curve in this plot with the correct slope, m_{PF}

$$m_{PF} = \frac{e_0}{k_B T}\left(\frac{e_0}{\pi\,\varepsilon_{r,opt}\varepsilon_0}\right)^{1/2}. \quad (3b)$$

From the slope, the optical dielectric constant, $\varepsilon_{r,opt}$, of the tested material can be extracted at fixed temperature! Unfortunately, many authors applying this fitting in the PF-plot even did not check the slope of their fitting curve. And those who did have to acknowledge in many cases that the slope is not consistent with the correct optical dielectric constant of their measured thin film material although $\varepsilon_{r,opt}$ often may not be known exactly for the used materials because, e.g., the production conditions of the thin films. These facts are also motivation for the study presented in this paper.

The higher the barrier of the trap for escape, Φ_t, i.e., the deeper its energy level, E_t, in the gap, the higher is its probability to have a trapped carrier. In general, the trap occupancy is regulated by the Fermi-Dirac-statistics[10] via the quasi-Fermi levels for electrons and holes, E_{fn} and E_{fp}, respectively: If the energy level of an electron trap, E_{tn}, lies between E_{fn} and the conduction band edge, E_C, ($E_{fn} < E_{tn} < E_C$) the probability for trapping and thus its occupancy is low and the trap is mostly empty and therefore charged due to the neutrality definition above. Such traps are called "shallow." In contrast, if E_{tn} is smaller than E_{fn} ($E_{tn} < E_{fn}$) the trapping probability and thus the occupancy is high. Such traps are called "deep" and they are mostly neutral. As this behavior, the occupancy with an electron and the charge state is very similar to that of a donor, such traps may be called "donor-like." Actually, the occupation probability for the electron trap is the same as that for the non-ionization of donors. Similarly, hole trapping centers may be called "acceptor-like" for the same reasons. The above described characteristics are schematically sketched in Fig. 2 for electron traps (left part) and hole traps (right part). The change of the trap energy level E_t by $\pm\Delta\Phi_{PF}$ changes the energy distance to the respective quasi-Fermi level and thus the trapping probability for the PFE. These changes in the trapping energy due to the PFE are implemented in the simulation tool described in Section "Simulation Tool And Variation of Parameters."

SIMULATION TOOL AND VARIATION OF PARAMETERS

The simulation tool used for the data reported in this paper has been used before to successfully reproduce experimental leakage current curves in wide band gap semiconductors such as $SrTiO_3$ (STO) and (Ba,Sr)TiO_3 (BST) with respect to dependencies on electric voltage (field), temperature, and film thickness.[4,5,11] As the features of the simulation program have been described in detail,[3–5] only a short recapitulation of the main characteristics is presented here with the help of Fig. 3, a schematic band diagram of a MIM stack with a wide band semiconductor.

The most important feature of this combined simulation tool is the condition for the currents in steady-state: The injection current density at one interface is identical to the current density inside the semiconductor film and identical to the ejection current density at the opposite interface

$$j_{n,p}(injection) \equiv j_{n,p}(film) \equiv j_{n,p}(ejection). \quad (4)$$

This identity holds for both carriers, electrons (n), and holes (p), and, of course, for the sum, the total current density j, which is plotted in the results section below. For the injection/ejection current densities, the thermionic emission, including the barrier reduction by the Schottky effect, is used. The current densities inside the film are described by drift and diffusion. The condition to equalize the currents at the interfaces has been suggested by Crowell, Sze, and coworkers,[1,2] also referenced as "Thermionic Emission—Diffusion Theory" in the textbook of Sze.[12] In thermal equilibrium, the Fermi levels on both sides of the interface are equal with no net current flowing. This is a dynamical balance of equal currents from the electrode (M) into the insulator (I), $j_{M\to I}$, and from insulator into the electrode, $j_{I\to M}$. For a flowing net current at an interface, which is a non-equilibrium state, the current is described by a difference in carrier densities, e.g., for the interface at $x = 0$ and electrons (n)

$$j_{n,injection} = e_0\Delta n(x=0)v_{r,n} = e_0[n_0(x=0) - n(x=0)]\,v_{r,n}, \quad (5a)$$

$$(\equiv j_{n,film}(\text{drift} - \text{diffusion}) \equiv j_{n,ejection}(x=d)(\text{thermionic emission})). \quad (5b)$$

For the case $n_0 > n$, there is an injection current from the electrode into the insulator, for the opposite case $n_0 < n$ the net current leaves the insulator into the electrode, here called ejection. $n_0(x=0) = N_C \exp[e_0\Phi_{Bn}(x=0)/k_BT]$ is the

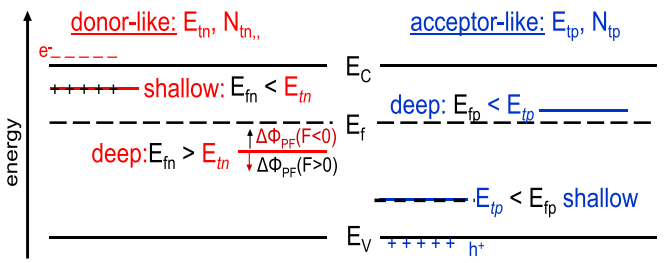

FIG. 2. Schematic sketch of shallow and deep donor-like and acceptor-like trapping centers within the band gap.

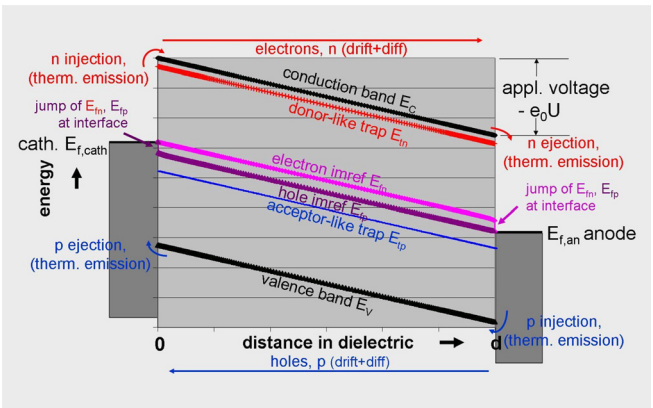

FIG. 3. Schematic sketch of a band diagram for the combined model used for simulation.

electron density in the equilibrium state, fixed by interface injection barrier, $\Phi_{Bn}(x=0)$, which is the difference between the bottom of the conduction band, $E_C(x=0)$, and the electrode Fermi level, $E_{f,electr}$, i.e., $e_0\Phi_{Bn}(x=0) = |E_C(x=0) - E_{f,cath}(x=0)|$. $n(x=0)$ is the electron density for the non-equilibrium state (with net current) in the first sheet of the semiconductor film at the interface $x=0$ and it is adjustable to assure the equality of the injection with the drift/diffusion current in the film, i.e., it is an adjustable boundary condition for the carrier (here: electron) density changing during the iteration process of the simulation program. The same applies to $n(x=d)$ at the ejection interface at $x=d$.

The term $e_0\ n_0(x=0)\ v_{r,n}$ is in the simplest case the usual (Schottky) current of thermionic emission with $v_{r,n} = A^*T^2/e_0N_C$ (the so-called recombination velocity for electrons).[12] N_C is the effective density of states at the bottom of the conduction band, A^* is the effective Richardson constant for thermionic emission. Similar equations as Eq. (5a) have been applied to injection and ejection for electrons and holes at both interfaces at $x=0$ and $x=d$, as indicated in Fig. 3.

The adjustable density $n(x=0)$ can also be related to a Fermi level with the equation $n(x=0) = N_C \exp\{\lfloor E_C(x=0) - E_{fn}(x=0)\rfloor/k_BT\}$. If $n \neq n_0$, i.e., if a net current is flowing, it follows $E_{fn}(x=0) \neq E_{f,cath}(x=0)$. This gives rise to a jump of the electron Fermi level for electrons at the cathode and in general at both interfaces for both kind of carriers and non-equilibrium quasi-fermi levels for electrons, E_{fn}, and holes, E_{fp}, respectively, inside the film, called Imrefs, as shown in Fig. 3.

It is also worth to mention another boundary condition for the solution of the drift-diffusion equation[4,13]

$$U = (k_BT/e_0)\ln[n_0(x=0)/n_0(x=d)] + \int_0^d dx F_{ext+int}(x). \quad (6)$$

The applied voltage U is divided into two terms: The first one is called diffusion voltage, the second drift voltage representing the acting electrical potential difference for the band conduction of the carriers. Due to this condition, the resulting working field in the dielectric can be very different from mean applied field, $F_{appl} = U/d$ because of the diffusion voltage and the internal field due to space charge using the Poisson equation. Especially, the field values at the interfaces are important because they determine via the Schottky effect the effective barriers for carrier injection/ejection.

Besides the mentioned limits of the energy bands, conduction band, E_C, and valence band, E_V, and the quasi-fermi levels, E_{fn} and E_{fp}, there are the important trap energy levels within the band gap, E_{tn}, and E_{tp}, respectively, which are both for shallow traps in Fig. 3, i.e., the traps are mostly without trapped carriers and therefore charged. The internal field due to the total space charge via the Poisson equation is small in the example compared to the mean applied field, $F_{appl} = U/d$ (applied voltage U divided by film thickness d), as the energy bands are nearly straight lines without significant bending. As the model describes injection of electron and holes (double injection), recombination reactions between the two species may be important. Generally, this effect is included in the simulation tool, but it has been verified that this process is only important if the injection currents and then the densities for both are about comparable, which for wide band gap thin film semiconductors is only true if the electrode Fermi levels are close to the middle of the gap. In this case, the injection currents and therefore the steady state current without recombination are already immeasurably small, so that the recombination effect was not included in the presented simulation results.

Only one additional paper is known to the author using a similar simulation model to explain experimental data.[14] It should be mentioned that a very similar model using tunneling injection instead of thermionic emission for the interface part has been applied by Baniecki and co-workers.[15,16] Other combined models, different from the used one, are reported in the literature, but as they differ in boundary conditions, often very significantly, they are not mentioned here, because a thorough discussion on the differences is beyond the scope of this paper. The reader is referred to textbooks, similar to Refs. 9 and 10.

The combined model shows very different current simulation curves varying in shape and profile and absolute number dependent on interface properties (electrode barrier height, electrode symmetry, etc.), film properties (permittivity, carrier mobility, thickness), film defect properties (width (homogeneity), energy level in the gap with respect to the Fermi level (shallow, deep) and type (donor-like, acceptor-like)) and temperature. The numbers for the varied parameters used for the simulations are listed in Table I: electrode properties (zero voltage barrier height symmetric for both interfaces), insulator properties (thickness, dielectric permittivity) and defect properties (density and energy level of donor-type and acceptor-type traps, respectively), and external properties (applied voltage (field), temperature). The simulation tool includes several temperature dependent parameters: diffusion constants and mobilities for electron and holes, respectively, and the semiconductor gap width as it is known that the gap width shrinks with increasing temperature: $E_g(T) = E_{g,T=0} - \beta T$ with $\beta = 6\times10^{-4}$ eV K^{-1}. The energy levels of the traps in the gap, E_{tn} and E_{tp}, and the top of the valence band, E_V, were adjusted accordingly, but in

TABLE I. Parameters for simulation calculations. Fixed parameters: Gap width $E_g = 3.3$ eV; relative optical (high frequency) dielectric const. $\varepsilon_{r,opt} = 5.5$; eff. density of states (DOS) conduction band: $N_C = 3.5\times10^{20} = N_V$: eff. DOS valence band.

Varied parameters	Units	Standard	min.	max.
Applied voltage, V	V		10^{-4}	25
Dielectric film thickness, d	Nm	30	15	250
Applied electric field, $F = V/d$	V/cm		4	2×10^6
Temperature, T	K	300	250	455
Relative dielectric constant, ε_r	…	30	10	300
Sym. interface barrier, Φ_{Bn} (Φ_{Bp})	V	0.3 or 1.0	0.15	3.0
Donor-like trap energy, E_{tn}	eV		0.05	2.0
Donor-like trap density, N_{tn}	cm^{-3}	10^{20}	10^{19}	3×10^{20}
Acceptor-like trap energy, E_{tp}	eV		0.9	3.0
Acceptor-like trap density, N_{tp}	cm^{-3}	10^{20}	10^{19}	3×10^{20}

figures and tables the nominal values (for $T=0$) are given if not mentioned otherwise. Many of the input numbers for the simulation program (mobilities, diffusion constants, effective densities of states in conduction and valence bands, etc.) have been adjusted for STO material (as it was used in previous papers). The most important are given here.

The gap width $E_{g,T=0}=|E_C-E_V|=3.3\,eV$ and hence $E_g(T=300\,K)=3.12\,eV$; the electron affinity, $\chi=4\,eV$; these two data together with the varied electrode Fermi level, $E_{f,electr}$, define interface barriers for electrons and holes, $e_0\Phi_{Bn}$, and $e_0\Phi_{Bp}=|E_V(x=0)-E_{f,cath}(x=0)|$ at the cathode, $x=0$, and at the anode, $x=d$, respectively, for zero electric field, i.e., without consideration of the Schottky effect. The effective density of states in conduction and valence band were chosen equal: $N_C=N_V=3.52\times10^{20}\ cm^{-3}$; a similar value is also used as upper limit for the density of traps. The effective Richardson constant, $A^*=983\,A/(cm\,K)^2$. The relative optical (high frequency) permittivity (relative optical dielectric constant), $\varepsilon_{r,opt}=5.5$. Due to these choices, the absolute numbers of calculated current density may change with the exact input numbers for other materials, but not the general results.

Of course, the simulation delivers current densities of any magnitude. But applied to experimental data there is an upper limit, because for higher current densities the sample would be damaged or completely destroyed by melting, and a lower limit, because of a resolution limit for current measurement. Assuming for the last 10^{-14} A, a very optimistic current resolution limit, the lower limit for the current density is dependent on the electrode area of the sample. This is listed in Table II. As most of the presented data are shown in a PF-plot, i.e., $\ln(j_{PF}/F_{appl})$ vs. $F_{appl}{}^{1/2}$, the resolution limit for j_{PF}/F_{appl} is also dependent on the applied electric field, F_{appl}. In Table I, this is shown for 3 V for a dielectric film thickness $d=30$ nm, the standard thickness for the simulations, resulting in a representative electric field of 1 MV/cm (or 1000 $[V/cm]^{1/2}$ in the PF-plot). For other conditions, the respective lower limits for j/F can easily be calculated. Although many of the presented data are smaller than the realistic current limits, they are shown for completeness and to confirm the drawn conclusions.

This powerful simulation tool was used to check if and to what amount the implementation of the PFE (as described before) would change the leakage current curves and if the possibly changed dependencies would show the characteristic slope in a PF-plot, as it is claimed in hundreds of papers.[6]

TABLE II. Current limit to be measurable.

Current $I>10^{14}\,A=10\,fA$	
Electrode area	Limit j/F [A/Vcm] at 1 MV/cm (i.e., 3 V for d = 30 nm)
$1\,cm^2$	$>10^{-20}$
$1\,mm^2$	$>10^{-18}$
$10\times10\,\mu m^2$	$>10^{-14}$
$1\,\mu m^2$	$>10^{-12}$
$30\times100\,nm^2$	$>3\times10^{-10}$
$30\times30\,nm^2$	$>10^{-9}$

RESULTS AND DISCUSSION

This section is divided into two parts: In the first one, the results are presented for simulations for which it was assumed that only a single type of trap is present, donor-like *or* acceptor like. In the second part, all the simulations results have as input both kinds of traps, which is called compensation of traps. As it should be demonstrated if and under which conditions the PFE is the dominating mechanism for the current density, nearly all the data are presented in the "PF-plot," i.e., $\log(j/F)$ vs. $F^{1/2}$. For comparison to the simulation results also the theoretical curve of the PFE (see Eq. (3a)) is plotted and usually normalized to high field data of one of the simulation curves with implemented PFE. In several plots, the simulation results with implementation of the PFE are compared to those without consideration of the PFE. These are labeled "w PF" and "w/o PF" and usually plotted as symbols without lines and lines without symbols, respectively, if not mentioned otherwise.

A. Single type of traps

For the simulation with only donor-like traps, a screening with varied energy level, E_{tn}, of the traps in the gap has been performed. E_{tn} is the absolute value below the conduction band edge, E_C, and measured in eV. Fig. 4(a) shows the comparison with and without PFE implementation in a PF-plot. The other parameters were the zero-field interface barrier for electrons, $e_0\Phi_{Bn}=1\,eV$, the donor-like trap density, $N_{tn}=2\times10^{19}\ cm^{-3}$, the relative dielectric constant, $\varepsilon_r=300$, and the film thickness, $d=30$ nm. In general, the effect of PFE implementation is negligible for most results. One can observe two "master curves," one with higher current for those with $E_{tn}<e_0\Phi_{Bn}$ and another one with $E_{tn}>e_0\Phi_{Bn}$ with lower current. The exception is for $E_{tn}=1\,eV$, the same value as $e_0\Phi_{Bn}$. With PFE, the curve joins those with $E_{tn}<e_0\Phi_{Bn}$ at high applied fields which is reasonable because the PFE reduces the trap energy level towards E_C. Without PFE, the curve joins those with $E_{tn}>e_0\Phi_B$ at high fields. None of the curves shows the slope characteristic for PFE represented by the "PF Theory" line.

Fig. 4(b) shows the results for a similar screening with a single acceptor-like trap with a density $N_{tp}=2\times10^{19}\ cm^{-3}$ and at varied energy level, E_{tp}. The energy level, E_{tp}, was also changed systematically from close to the valence band ($E_{tp}=3.15\,eV$) to deep in the gap ($E_{tp}=1.0\,eV$), while all other parameters were identical to the previous donor-like trap screening. [Note: The numbers for E_{tp} are measured as absolute values below the bottom of the conduction band, E_C. If measured above top of the valence band, they are labeled $E_{tpv}=|E_g-E_{tp}|=|3.3-E_{tp}|$]. The results are very similar: Only for the case that $E_{tp}\cong e_0\Phi_{Bn}$ (or $E_{tpv}\cong e_0\Phi_{Bp}$), there is a difference with and without PFE implementation, but both are far away from the theory line. All other curves make a "master curve," because in the band gap all other $E_{tp}>e_0\Phi_{Bn}$ (or $E_{tpv}<e_0\Phi_{Bp}$). Although this master curve in the average is close to the PF theory, it is no indication for the PFE because the curves without PFE implementation are identical and at high applied fields, the main range for the PFE, the slope is significantly different from the theory.

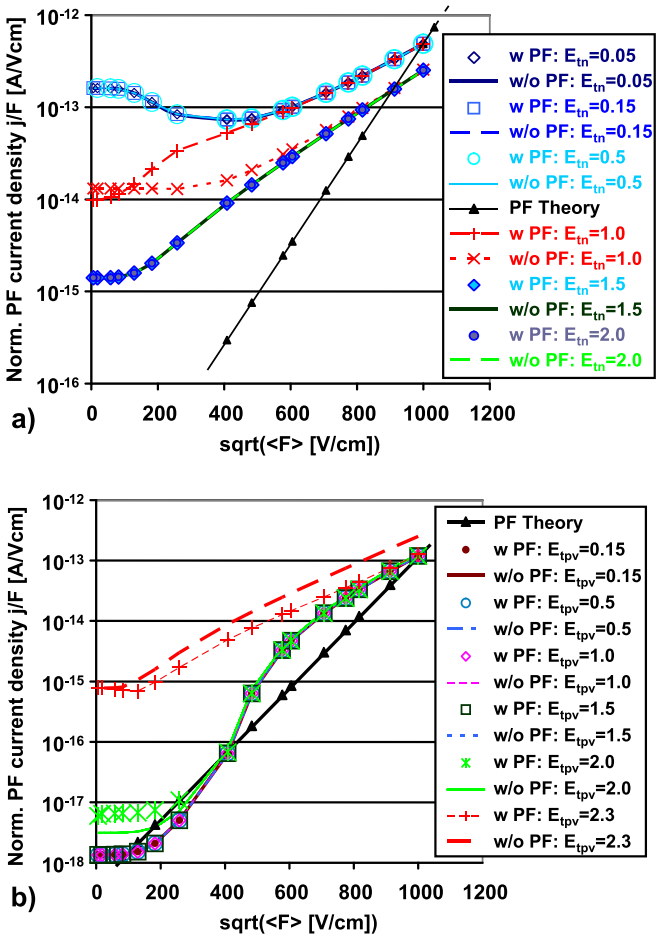

FIG. 4. Comparison of simulation data (PF-plot) without (w/o) and with (w) implementation of PFE: (a) for donor-like traps with density $N_{tn} = 2 \times 10^{19}$ cm^{-3}, varying trap energy level E_{tn} [eV] and (b) for acceptor-like traps with density $N_{tp} = 2 \times 10^{19}$ cm^{-3}, varying trap energy level E_{tpv} [eV]. The nominal interface barriers were the same for both cases, $e_0\Phi_{Bn} = 1$ eV, which corresponds to $e_0\Phi_{Bp} = 2.3$ eV (measured above E_V). The other parameters are mentioned in the text.

Many other simulations with single traps only have been performed in the parameter ranges listed in Table I. Some data for donor-like traps are presented in Fig. 5 for those examples with one or more parameters at the limit of the investigated ranges. All these shown curves with implemented PFE are very different from the respective ones without PFE which are not shown. Except for one example all the simulations are made with $E_{tn} = e_0\Phi_{Bn} = 1$ eV similar to those in Fig. 4(a). The closest approach to the slope of the PFE theory shows the curve with $\varepsilon_r = 10$, $d = 80$ nm, and $N_{tn} = 10^{20}$ cm^{-3}. Fitting the slope of this curve (see Eq. (3b)) and extracting the optical dielectric constant, $\varepsilon_{r,opt}$, results in a value of 9.6 instead the correct input of 5.5. For the others, the difference would be much larger. Using smaller interface barrier height and lower trap energy level (here: $e_0\Phi_{Bn} = 0.3$ eV and $E_{tn} = 0.5$ eV), the current density increases significantly, but also for this example the slope is for off from PF theory.

The results for single donor-like traps with trap energy equal to the interface barrier, $E_{tn} = e_0\Phi_{Bn} = 1$ eV, are summarized in Fig. 6 with respect to the three most important parameters: relative dielectric constant, ε_r (Fig. 6(a)),

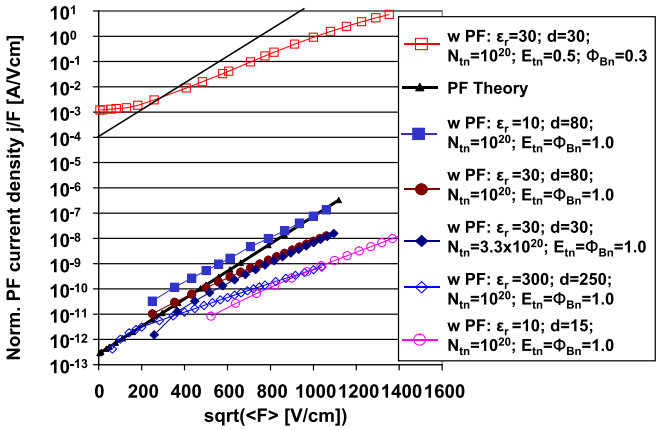

FIG. 5. Comparison of simulation data (PF-plot) with (w) implementation of PFE for donor-like traps with different numbers for relative dielectric constant, ε_r, dielectric film thickness, d [nm], trap density, N_{tn} [cm^{-3}], trap energy level, E_{tn} [eV], and nominal interface barrier, $e_0\Phi_{Bn}$ [eV]. The other parameters are mentioned in the text.

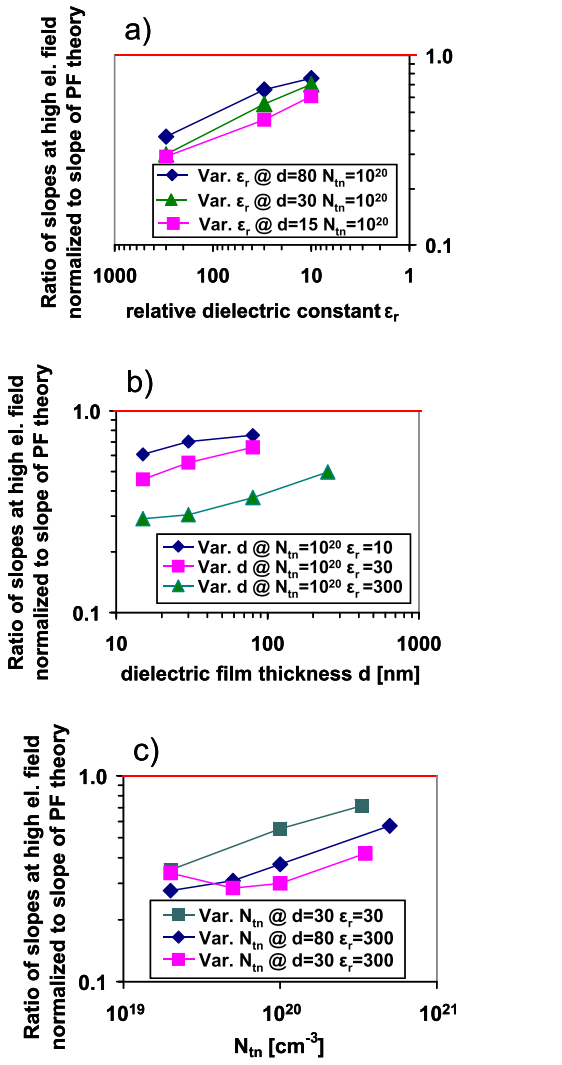

FIG. 6. Summary of simulation data for single donor-like traps present only. Plotted is the slope of the current–field curves in the PF-plot, normalized to the theoretical slope expected for PFE as dominating conduction mechanism vs. important parameters: (a) relative dielectric constant, ε_r; (b) dielectric film thickness, d [nm]; (c) trap density, N_{tn} [cm^{-3}]. The other parameters are mentioned in the legend or the text.

dielectric film thickness, d (Fig. 6(b)), and trap density, N_{tn} (Fig. 6(c)). Plotted are the slopes at high applied fields of the simulation curves in the PF-plot, normalized to theoretical slope of Eq. (3a) (which is then equal to 1). The trends in the figures are clear: with decreasing ε_r, and increasing d and N_{tn} the data get closer to the theoretical value, but the distance to that value is still significant. The closest approach, as mentioned above, for $\varepsilon_r = 10$, $d = 80\,\text{nm}$, and $N_{tn} = 10^{20}\,\text{cm}^{-3}$ is at about 75%.

Similar data could be shown for curves with single acceptor-like traps. So the main conclusion is that the PFE dominated behavior has not been verified within the parameter field tested for single traps present only. This makes the PFE as dominating mechanism for currents through MIM stacks improbable under these conditions.

B. Both types of traps (compensation)

For this condition, a parameter screening was done, similarly as for single traps above, and the results are shown in Figs. 7(a) and 7(b). For the data in Fig. 7(a), the value of the symmetric interface barrier, Φ_{Bn}, was shifted through the band gap for the constant parameter set $N_{tn} = N_{tp} = 2 \times 10^{19}$ cm^{-3} (exact compensation), $E_{tn} = 0.15\,\text{eV}$ (shallow), $E_{tp} = 2.0\,\text{eV}$ ($E_{tpv} = 1.3\,\text{eV}$); deep or shallow), $d = 30\,\text{nm}$, and $\varepsilon_r = 300$. As expected, the absolute magnitude of the current is very dependent on the distance of the electrode Fermi level $E_{f,electr}$ from the conduction or valence band, respectively, and therefore on the respective barrier heights at the interfaces, $e_0\Phi_{Bn}$ for electrons and $e_0\Phi_{Bp}$ for holes, whatever is smaller. At high applied fields, all curves are rather far off from the slope of the PFE theory. The comparison between with and without PFE implementation shows no significant difference except for the case $E_{tpv} = e_0\Phi_{Bp} = 1.3\,\text{eV}$ (or $E_{tp} = 2.0\,\text{eV}$) for which a small difference appears.

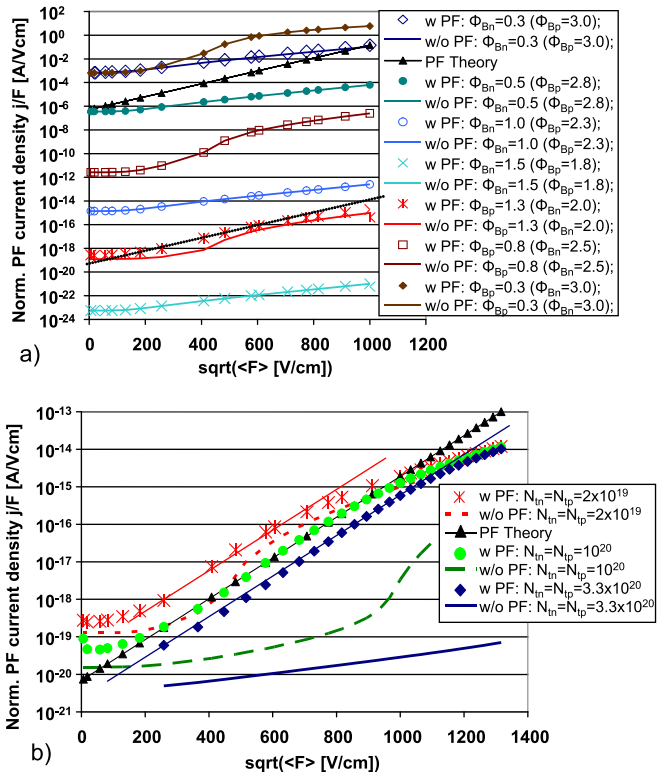

FIG. 7. Comparison of simulation data (PF-plot) without (w/o) and with (w) implementation of PFE for exactly compensated traps at constant parameters (see text) except: (a) the symmetric interface barrier was varied and shifted through the whole gap; (b) the densities of the traps $N_{tn} = N_{tp}$ were varied for the parameter set, which showed a dependence on the PF-implementation in Fig. 7(a).

For this condition, a dependence on trap density with exact compensation was made. The results are plotted in Fig. 7(b). With increasing trap density, the field range, in which the slope of the curve is close to that of PFE theory, increases. This does also the difference compared to the curves without PF implementation. All the curves with PF implementation drop in slope at very high fields and leave the theory curve but the onset field for this deviation increases with increasing N_t, too. Therefore, also other parameters than trap density, N_t, were changed under the condition of exact compensation.

In order to increase the current density, smaller interface barriers for electrons, $e_0\Phi_{Bn}$, with similar energy level of donor-like traps, E_{tn}, and identical conditions for holes and acceptor-like traps, respectively, were tested. The optimum results for the electron case are shown in Fig. 8(a). The

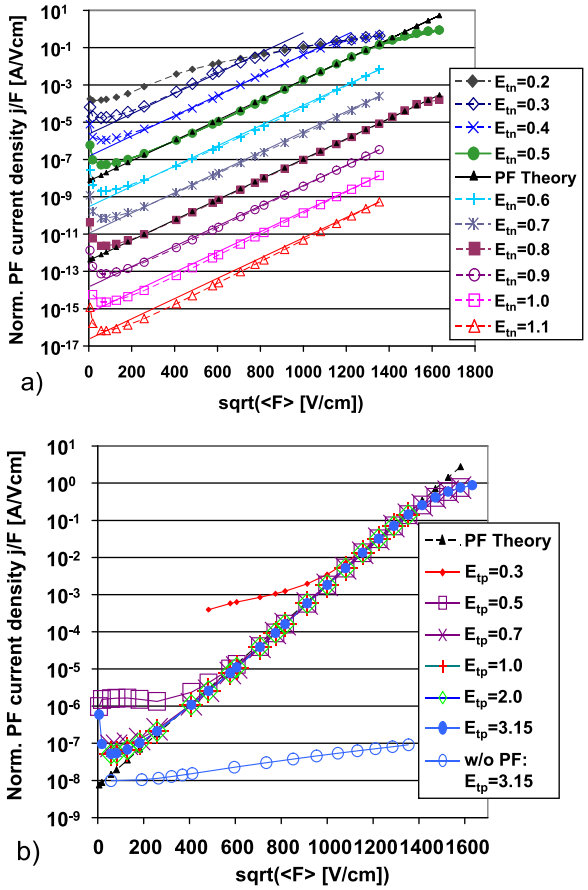

FIG. 8. Comparison of simulation data (PF-plot) with implementation of PFE (if not indicated otherwise) for exactly compensated traps at constant parameters (see text) except: (a) the energy level of the donor-like traps, E_{tn}, which was varied from weakly deep to strongly deep; (b) the energy level of the acceptor-like traps, E_{tp}, which was varied from strongly deep to weakly deep for the parameter set for the curve with $E_{tn} = 0.5\,\text{eV}$ in Fig. 8(a). The straight lines for each curve correspond to the expected PFE theory normalized at high applied fields.

parameters were: $N_{tn} = N_{tp} = 10^{20}\,cm^{-3}$ (exact compensation), $e_0\Phi_{Bn} = 0.3\,eV$ (i.e., $e_0\Phi_{Bp} = 3.0\,eV$), $E_{tp} = 3.15\,eV$ ($E_{tpv} = 0.15\,eV$; shallow), $d = 30\,nm$, and $\varepsilon_r = 30$. The varied parameter was the trap energy, E_{tn}, from very small, 0.2 eV (shallow), to 1.1 eV (deep) in steps of 0.1 eV. For $E_{tn} = 0.2\,eV < e_0\Phi_{Bn}$, the curve does not fit the PFE theory. The curve for $E_{tn} = 0.3\,eV$ ($=e_0\Phi_{Bn}$) is close to it at medium applied fields, but in the high field range the slope decreases strongly. For $E_{tn} = 0.4\,eV$ ($>e_0\Phi_{Bn}$), the curve is very close to PFE theory, only at very high fields the slope decreases. For the range $0.5\,eV \le E_{tn} \le 0.8\,eV$ (all $E_{tn} > e_0\Phi_{Bn}$), the fit to the PFE theory is almost perfect except for very low fields, for which the PFE is not expected to work anyway, and a bending at the highest fields applied. For higher E_{tn} up to 1.1 eV, the slopes are close to theory but get steeper than theory with increasing E_{tn}. These data of an electron-conduction dominated current with exact compensation at high trap density with the donor-like trap energy E_{tn} about 0.2 to 0.5 eV lower in the gap than the electron interface barrier, $e_0\Phi_{Bn}$, are the first and only reported results up to here that show the theoretical PFE behavior. Therefore, it was tested if changes in the other parameters would save or destroy the found PFE behavior and some examples are shown in Figs. 8(b), 9, and 10.

For one of the curves in Fig. 8(a) ($E_{tn} = 0.5\,eV$), the energy level for the compensating acceptor-like traps, E_{tp}, was changed from the very shallow value $E_{tp} = 3.15\,eV$ ($E_{tpv} = 0.15\,eV$) more into the gap in steps up to the value $E_{tp} = 0.3\,eV = e_0\Phi_{Bn}$, the interface barrier for the current dominating electrons. The results are plotted in Fig. 8(b). Except for the curve with the smallest value of E_{tp}, its variation does not change the PF behavior and all the curves coincide in the high field range. The curve with $E_{tp} = 0.5\,eV$ leaves the PF theory curve at medium fields. For the one with the smallest E_{tp} (=0.3 eV), the deviation occurs already in the upper field range so that it would be difficult to observe the PFE behavior in reality under these conditions,

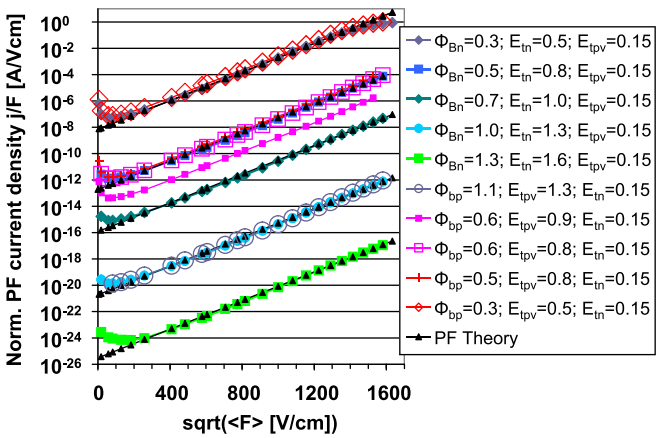

FIG. 9. Comparison of simulation data (PF-plot) with implementation of PFE for exactly compensated traps at constant parameters (see text) except pairs of the energy level of the traps for the current dominating carrier, E_{tn} for electrons or E_{tpv} for holes, and the corresponding interface barrier, Φ_{Bn} for electrons or Φ_{Bp} for holes, respectively. The straight lines with the triangles for each curve correspond to the expected PFE behavior normalized at high applied fields.

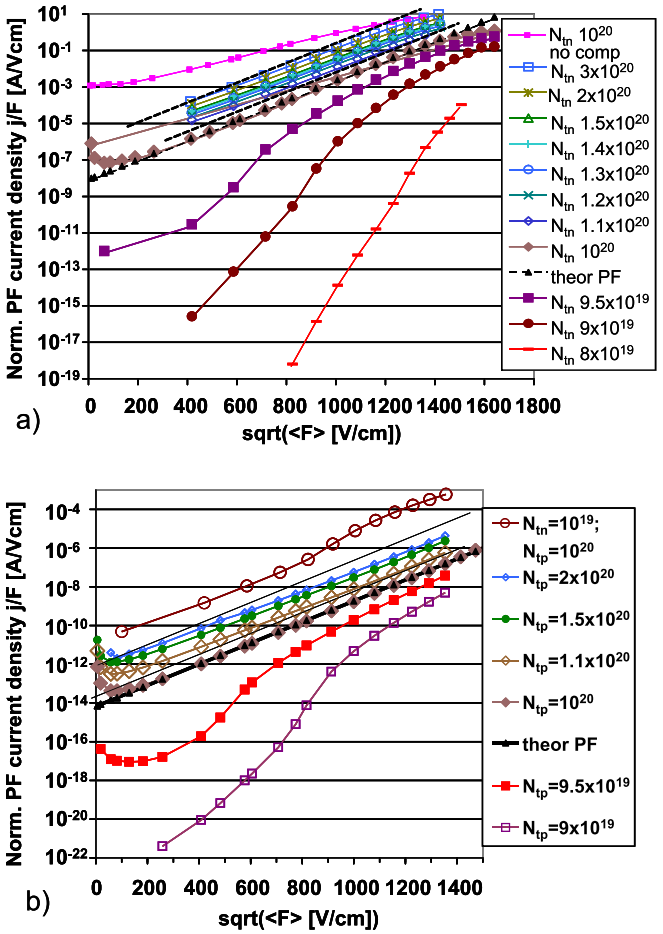

FIG. 10. Comparison of simulation data (PF-plot) with implementation of PFE for nearly compensated traps at constant parameters (see text) except: (a) the density of donor-like traps, N_{tn}, which was varied around the constant density of the acceptor-like traps, $N_{tp} = 10^{20}\,cm^{-3}$ from over-compensation, $N_{tn} < N_{tp}$ (lower curves) to under-compensation, $N_{tn} > N_{tp}$ (upper curves) for electron dominated current, and (b) the density of acceptor-like traps, N_{tp}, which was varied around the constant density of the donor-like traps, $N_{tn} = 10^{20}\,cm^{-3}$ from over-compensation, $N_{tp} < N_{tn}$ (lower curves) to under-compensation, $N_{tp} > N_{tn}$ (upper curves) for hole dominated current. In each figure, one curve with high under-compensation was added for comparison. The straight lines for selected curves correspond to the expected PFE behavior normalized at high applied fields.

also because at very high fields all the curves deviate increasingly from the PF slope. For comparison, a simulation result for one of the cases without PFE implementation is plotted as well, showing a very different behavior in slope and absolute value which is true for all the other cases as well. In conclusion, the energy level E_{tp} of the acceptor-like traps does not influence the observation of the PFE as long as E_{tp} is lower than the respective Fermi level, i.e., the acceptor-like trap has always to be shallow.

The rule that PFE behavior may be observed for the exactly compensated traps if E_{tn} is about 0.2 to 0.5 eV larger than $e_0\Phi_{Bn}$ and E_{tp} not smaller than $e_0\Phi_{Bn}$ has been verified in the previous figures. Similar combinations have been investigated by shifting the interface barrier $e_0\Phi_{Bn}$ deeper into the gap inducing lower, eventually unrealistic low current densities. For $\Phi_{Bn} > \Phi_{Bp}$, resulting in hole dominated currents, E_{tp} for acceptor-like traps was varied instead of E_{tn}, which was then chosen constant and shallow at 0.15 eV. The

results, plotted in Fig. 9, demonstrate that under these conditions, i.e., Φ_{Bn} and Φ_{Bp} deeper in the gap, nearly perfect PF behavior is observed, even better than the starting curve at the top of the plot, as no deviation from PFE theory occurs up to the highest applied fields tested in the simulations, other than for $e_0\Phi_{Bn} = 0.3$ eV and $e_0\Phi_{Bp} = 0.3$ eV. The drawback of the higher barriers is the much lower current density, so that the lowest 2 or 3 curves are hardly measurable in reality.

The assumption of *nominally identical densities* of donor-like and acceptor-like traps in all the previously shown simulation results in this section is rather unrealistic. Therefore, the effect of small deviations from this exact compensation was tested for both directions, under-compensation as well as over-compensation with respect to N_{tn} for constant $N_{tp} = 10^{20}\,cm^{-3}$ and variations of N_{tn} around this number. The other parameters are the same as in the figures before with $e_0\Phi_{Bn} = 0.3$ eV, $E_{tn} = 0.5$ eV, and $E_{tp} = 3.15$ eV. The results are shown in Fig. 10(a).

All the curves with under-compensation, $N_{tn} > N_{tp}$, lie above the reference curve with exact compensation, these with over-compensation, $N_{tn} < N_{tp}$, lie below. The curves with under-compensation are nearly straight lines in this PF-plot, but the slope decreases already noticeably for 10% under-compensation ($N_{tn} = 1.1 \times 10^{20}\,cm^{-3}$) compared to the reference curve and the PF theory curve. This decrease is enlarged by increasing under-compensation, and for highest number shown here, $N_{tn} = 3 \times 10^{20}\,cm^{-3}$ (i.e., $3 \times N_{tp}$), close to the upper limit for N_t, the curve gets additionally bended at high applied fields making the deviations more significant. This trend would be limited by the most extreme under-compensation ($N_{tp} = 0$; single donor-like trap only), the most upper curve in Fig. 5 with otherwise identical parameters except N_{tn}.

Over-compensation makes the deviations much more serious: a 5% over-compensation changes the curve already very drastically, only in a quite small range at high fields the slope is close to PF theory, while below and above this field range the slope of the curve is far off. This destruction of the PF behavior is complete already for a 20% over-compensation and in most of the field range the current is immeasurably small.

A similar plot is shown in Fig. 10(b) for hole dominated currents. The curve with exact compensation as reference is the same as in Fig. 9(b) with the parameters $e_0\Phi_{Bp} = 0.6$ eV; $E_{tpv} = 0.9$ eV, i.e., the barrier is higher than in the electron case (Fig. 10(a)) and also the difference of the acceptor-like trap energy level and the barrier level in order to present some variation of these parameters. The under- and over-compensation with respect to N_{tp} are similarly: shallow $E_{tn}(= 0.15$ eV below $E_C)$ and constant $N_{tn} = 10^{20}\,cm^{-3}$ and variations of N_{tp} around this number.

The results are nearly identical to the electron case (in Fig. 10(a)): All the curves for under-compensation, $N_{tp} > N_{tn}$, lie above the reference curve with exact compensation, these for over-compensation, $N_{tp} < N_{tn}$, lie below. For increasing under-compensation, the slopes of the nearly straight lines deviate increasingly from the PF theory. The largest under-compensation shown with a factor of 10 and $N_{tp} = 10^{20}\,cm^{-3}$, the most upper curve, does not fit the PF theory especially at high fields because it is bended. As in the electron case (Fig. 10(a)) already small over-compensation destroys the PF behavior completely.

Using some examples of the electron case, i.e., shallow $E_{tp} = 3.15$ eV and constant $N_{tp} = 10^{20}\,cm^{-3}$, $\Phi_{bn} = 0.3$ eV, $E_{tn} = 0.5$ eV and varying N_{tn} around N_{tp} (Fig. 10(a)), it is tried to understand the occurrence of the nearly perfect PF-behavior for exact compensation and the increasing deviation with increasing under-/over-compensation. The selection is shown in Fig. 11 (full symbols): Exact compensation (diamonds, middle curve), under-compensation ($N_{tn} = 3 \times 10^{20}\,cm^{-3}$; squares, upper curve), and over-compensation ($N_{tn} = 9 \times 10^{19}\,cm^{-3}$; circles, lower curve).

As one of the conditions for the observation of the PF-behavior is that the resulting current density is not limited by the (electron) injection via thermionic emission including the Schottky effect, additionally to the simulation results the corresponding maximum injection current densities (open symbols) are plotted. For their calculations, the *working* fields at $x = 0$, $F(x = 0)$ were used. In order to compare to the results of the simulation results in the PF-plot, the injection currents have been divided by the applied field, $F_{appl} = U/d$. All these injection current densities are larger than the simulation current densities, about a factor of two at high applied fields up to one order of magnitude or more at medium applied fields. Therefore, the simulation current densities are not limited by the injection—in this case, both current densities would be nearly equal, and this holds not only for the shown examples, but generally within the parameter range used in the reported results. It is worth to note that the shown maximum injection current densities are not the real ones in the simulation but corresponding to Eq. (5a) they are reduced to the simulation current densities by the "recombination" effect in the used model in order to satisfy Eq. (4). For comparison, the injection current density curve divided by F_{appl}

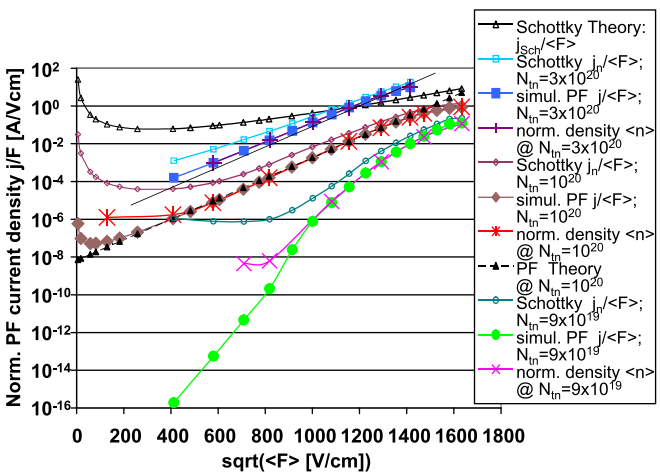

FIG. 11. Comparison of selected simulation data (PF-plot) of Fig. 10(a) (full symbols) with the corresponding maximum current of thermionic injection including the Schottky effect (open symbols) and the corresponding mean electron densities, $\langle n \rangle$, normalized to the currents at high applied field (crosses and star symbols). For comparison, the current of thermionic injection including the Schottky effect with the applied electric field, F_{appl}, has been added (most upper curve). The straight lines for selected curves correspond to the expected PFE behavior normalized at high applied fields.

(PF-plot!), using the *applied* field as working field at $x = 0$, $F(x = 0) = F_{appl}$, in the Schottky barrier reduction, is also plotted (open triangles). The mostly large differences between the injection current curves are due to the differences between F_{appl} and the calculated working field at $x = 0$ due to the applied boundary condition for the drift-diffusion equation in Eq. (6). The such determined *working* fields at $x = 0$ (and $x = d$) induce quite different Schottky barrier heights at the interfaces and consequently different maximum current densities for injection (ejection) as shown in Fig. 11 for the injection of electrons at the cathode.

Another condition for the observation of the characteristic PF dependence is extracted from Eq. (2): the PF conductivity σ_{PF} is only dependent on the electron carrier density n_{PF} as all other parameters are kept constant except the field, F_{appl}. Therefore, the dependence of $n_{PF}(F_{appl}{}^{1/2})$ should have the characteristic PF behavior to observe the correct slope in the PF plot. The mean values of the electron density in the simulation, $\langle n(x) \rangle$, have been evaluated and plotted in Fig. 11 (star and cross symbols), normalized to the high field data of the corresponding currents (at about 1300 $(V/cm)^{1/2}$, $U_{appl} = 5$ V). For the middle curve with nearly perfect PF behavior, also the mean electron densities show exactly the same dependence at high and medium fields, but deviate at smaller fields. But this perfect fitting is not an exclusive indication for correct PF behavior because similarly ideal fitting is also observed for the other examples in Fig. 11 in the same field range. This identical dependence is generally observed in the medium to high field range because diffusion currents, the second part in the drift-diffusion equation used for the carrier transport inside the dielectric, are increasingly unimportant under these conditions.

Unfortunately, no significant difference in relevant properties could be evaluated from the simulation data which could explain the occurrence of the nearly perfect PF behavior as shown in Figs. 8 and 9 and in the same way the deviations from it documented in Figs. 10(a) and 10(b). Therefore, the appearance of the nearly perfect PF behavior may be just by chance induced by the decreasing slope from over- to under-compensated with additional straightening of the curves in the PF-plot.

So far, the field dependence of the PF current density has been addressed at constant temperature ($T = 300$ K). The strong temperature dependence of the PF current density (see Eqs. (2) and (3a)) will be presented and discussed below. From such dependence, some information about the energy level of the current controlling traps, E_t, and therefore about its barrier for escape at zero field, $e_0\Phi_t$, can be extracted via the zero field conductivity, σ_0 (T). For the temperature variations, all the simulations were done for electron controlled current with donor-like electron traps at a fixed energy level $E_{tn} = 0.5$ eV below the conduction band independent on temperature. [Note: This is different from all other simulation data for which the energy levels of the traps were dependent on temperature because they were scaled with temperature in the same way as the gap width (see above); e.g., a nominal trap energy $E_{tn}(T = 0) = 0.5$ eV was scaled to $E_{tn}(T = 300) = 0.473$ eV.

The other simulation parameters for the temperature variation are the ones for exact compensation of the trap densities, $N_{tn} = N_{tp} = 10^{20}\,cm^{-3}$, as stated in the figure caption and the corresponding text for Fig. 10(a), for which the results showed nearly perfect PF behavior over a wide field range. The simulation results with varied temperature between 250 K and 455 K are shown in Fig. 12(a). In general, the current density is increasing with increasing temperature. All the curves (symbols) show a "linear" dependence in the PF plot over a wide field range. Deviations from this behavior occur at low fields and at very high fields. For the last the bending starts at lower fields with increasing temperature leading to a current density independent on temperature at the highest fields tested. At all temperatures, the field dependence in the "linear" section of the curves is very close to the one expected for perfect PF behavior, exemplified for $T = 300$ K (triangles). The straight lines in Fig. 12(a) are the least square fits of the "linear" PF regions at each temperature, which are nearly identical with the PF theory lines normalized to one data point at the respective temperature as it is demonstrated for $T = 300$ K.

The intersections of these lines with the abscissa are representing the zero field conductivities. The natural logarithm, $\ln[\sigma_0(T)]$, of these extracted values is plotted vs. 1/temperature (see Eqs. (2) and (3a)), shown in Fig. 13, symbols of middle curve. From the slope of the least square fit, the energy level of the current controlling trap, in this case a donor-like trap, can be calculated assuming PF behavior. The extracted trap energy, $E_t = 0.507$ eV below the conduction band limit, E_C, is very close to the simulation input of $E_{tn} = 0.5$ eV. This may be a possible indication for PF as dominating current mechanism in the medium field ranges, used for the extraction of σ_0 (see Fig. 12(a)), for the condition of exact trap compensation.

In order to test the effect of very small deviations from the exact trap compensation on the indicated nearly perfect PF behavior, we performed identical sets of simulation curves with field and temperature dependence with the only change from exact compensation to slightly under-compensation of 10% with $N_{tn} = 1.1 \times 10^{20}$ cm^{-3} and very slightly over-compensation of 1% with $N_{tn} = 9.9 \times 10^{19}$ cm^{-3}, both at steady $N_{tp} = 10^{20}\,cm^{-3}$. The results are plotted in Figs. 12(b) and 12(c) (symbols). The general trends are the same as in Fig. 12(a), increasing currents with increasing temperature and "linear" PF behavior in wide field regions. But there is already a significant difference between the slopes of PF theory (triangles) and the least square fit for the "linear" portion at $T = 300$ K for both cases. These deviations can be quantified by extracting the high frequency dielectric constant $\varepsilon_{r,opt}$ from the slope of the fitting curve, e.g., at $T = 300$ K for both cases: For the under-compensation (Fig. 12(b)), the extracted high frequency dielectric constant is $\varepsilon_{r,opt} = 6.2$, an increase of about 13% compared to the input of $\varepsilon_{r,opt} = 5.5$. For the case of over-compensation (Fig. 12(c)), the extracted high frequency dielectric constant is $\varepsilon_{r,opt} = 4.8$, a reduction of about 13% compared to the input of $\varepsilon_{r,opt} = 5.5$. Similar deviations are observed for all temperatures for the respective cases. The temperature dependences in Figs. 12(b) and 12(c) were also

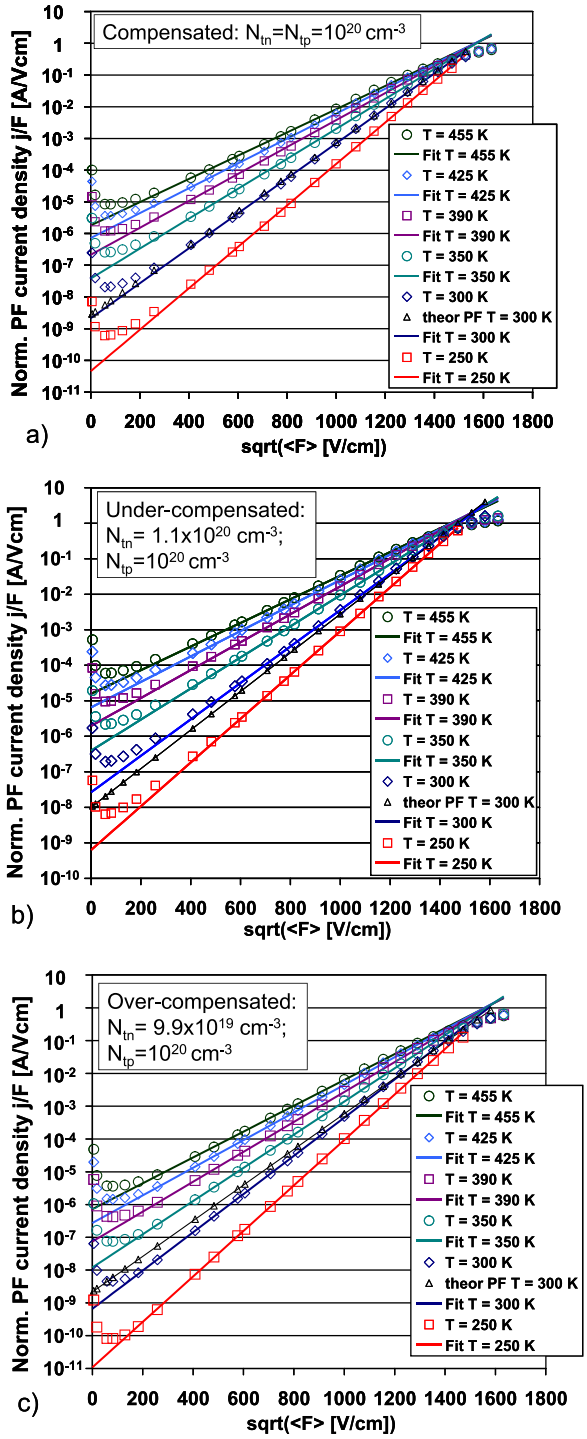

FIG. 12. Temperature dependence of simulation data (PF plot) with implementation of PFE. The input parameters are the same as for the data in Fig. 11 with exact compensation, except the fixed $E_{tn} = 0.5$ eV (see text): (a) with exact compensation, $N_{tn} = N_{tp} = 10^{20}$ cm^{-3}; (b) with 10% under-compensation, $N_{tn} = 1.1 \times 10^{20}$ cm^{-3}, $N_{tp} = 10^{20}$ cm^{-3}; (c) with 1% over-compensation, $N_{tn} = 9.9 \times 10^{19}$ cm^{-3}, $N_{tp} = 10^{20}$ cm^{-3}. The straight lines for each data are the least square fits, neglecting the data at very high and very low applied fields.

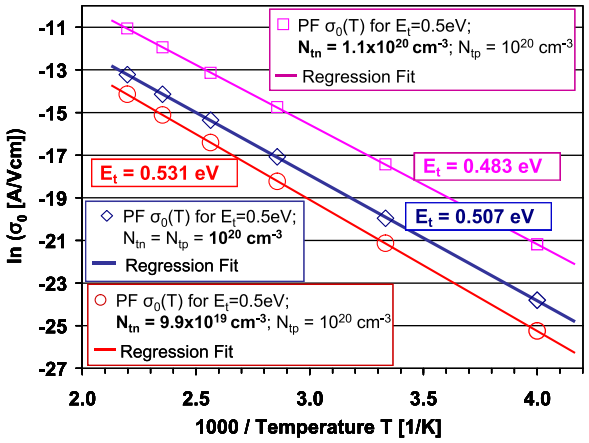

FIG. 13. Arrhenius plot for the zero field conductivity, σ_0, extracted from Fig. 12. The trap energy level, E_t, is extracted from the slope of the least square fit (straight line).

used to determine the respective trap energies via the numbers for $\sigma_0(T)$ extracted from the fitting lines. The results are plotted in Fig. 13 for under- and over-compensation, the symbols of the upper and lower curves, respectively. The extracted trap energies, $E_t = 0.483$ eV (Fig. 13, upper curve) and $E_t = 0.531$ eV (Fig. 13, lower curve), represent changes of about -3.3% and about $+6\%$, respectively, compared to the input of $E_{tn} = 0.5$ eV. These changes are less significant than those for $\varepsilon_{r,opt}$ also for real measurements because the exact trap energies are usually not known very well and they vary around a mean value. In conclusion, small deviations from the unrealistic condition of exact trap compensation result in much larger deviations from the perfect PF behavior, and this holds for all temperatures tested.

Some other effects, which are not included in the presented simulation model, may change the current-field dependence significantly and possibly destroy the PF behavior observed only for special conditions in the presented data.

At the interfaces, the carriers are injected or ejected not only by thermionic emission but could enter or leave the dielectric by tunneling into or from the conduction band for electrons or from valence band for holes, respectively. Although also these additional currents would be reduced by "recombination" in the model similarly as for thermionic emission, but they would increase the steady state current densities, especially at higher fields, the most important range for the PF, and possibly change the reported dependencies.

Only data for simulations with symmetric electrodes have presented in order to restrict the parameter range and, therefore, no dependence on the sign of the applied voltage is important. Compared to experiments, this assumption is not very appropriate for thin films, even if the electrodes are nominally identical, because due to the production conditions an interface M-I may be different from an I-M one even with the same materials for electrode (M) and dielectric (I). If the electrodes and hence the interface barriers are different, there will be a dependence on the sign of the applied voltage and the asymmetry itself can change the current-field dependence.

Another effect not included is illustrated in Fig. 14: In the simulation, the trap centers are treated as single, isolated traps without interaction with neighboring ones as shown in Fig. 1. This is the most upper (Coulomb) potential in Fig. 14 for the charged trap positioned at $x = 0$. For

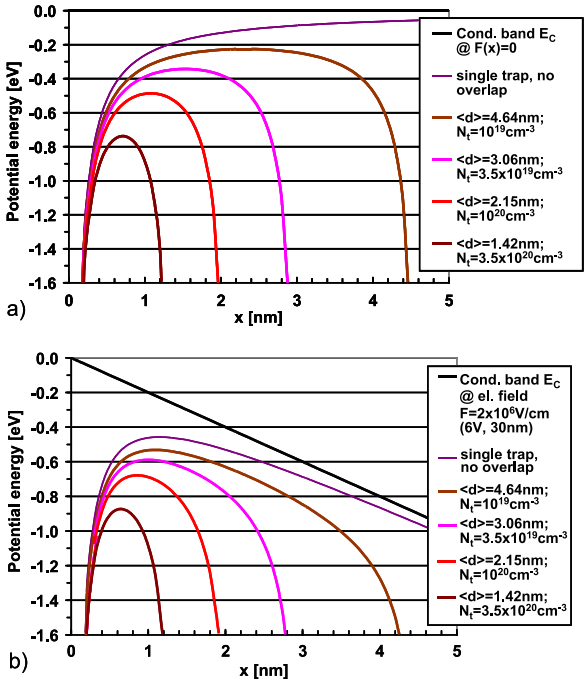

FIG. 14. (Coulomb) Potential overlap of neighboring charged traps for electrons. The first trap is fixed at $x = 0$, the second at the mean distance of the traps, $\langle d_t \rangle$, calculated from the densities, N_{tn}. (a) without electric field, $F = 0$; (b) with electric field, $F = 2 \times 10^6$ V/cm.

the high trap densities used in this report, this assumption is not really true as demonstrated in Fig. 14(a) without and in Fig. 14(b) with electric field, respectively. The first trap is positioned at $x_1 = 0$, the second at $x_2 = (1/N_t)^{1/3} = \langle d_t \rangle$, which is the mean distance between next neighbors of the traps.

For example, this distance is $\langle d_t \rangle = 2.15$ nm for the often used trap density of $N_t = 10^{20}\,\mathrm{cm}^{-3}$. Both traps are assumed to be charged and the neighboring Coulomb potentials overlap leading to a reduction of the barrier between the neighboring traps below the barrier to the conduction band (for electrons). At $\langle d_t > \rangle = 2.15$ nm ($N_t = 10^{20}\,\mathrm{cm}^{-3}$), there is no barrier for hopping between traps for all traps having energy levels $E_t \leq 0.5$ eV below the conduction band. This holds already for zero (or small) fields (Fig. 14(a)) and the barrier reduction increases with increasing field (Fig. 14(b)) and would apply to the selected examples in Figs. 10(a) and 11 with $E_{tn} = 0.5$ eV. That may result in additional hopping current contribution at all applied fields, of course depending on the occupation probability of the traps and their density compared to the carrier density in the respective band responsible for the presented data. For traps deeper in the gap also additional tunneling through the reduced barrier between neighboring trap centers may be significant especially for the highest trap density ($N_t = 3.5 \times 10^{20}\ \mathrm{cm}^{-3}$), for which the tunneling distance is mostly 1 nm or smaller.

CONCLUSIONS

The current through MIM thin film stacks in different wide band gap semiconductors was calculated using an advanced simulation tool, which combines injection/ejection currents at the MI interfaces with the drift-diffusion current inside the dielectric under the condition of an overall constant steady state current. The aim was to check the importance of the PFE as dominating conduction mechanism in such systems as it is suggested or "proved" in many publications.[6]

The currents without and with PFE implementation are compared in a wide parameter field for different trap configurations with respect to compensation, densities, and energy levels within the gap. For single traps present only, donor-like or acceptor-like, i.e., no trap compensation, an effect of the PFE implementation is only detected if the trap energy level is identical or very close to the injection barrier (electrode Fermi level), but in no case the current density curve shows the characteristic slope expected for a dominating PFE behavior.

With trap compensation, an effect of the PFE implementation is often confirmed, but nearly perfect PFE behavior is detected for *exact* compensation only, while deviations to under- or over-compensation destroy the PFE behavior, very dramatically for the last. The appearance of the nearly perfect PFE behavior in a wider range of the applied field is observed only for special parameter sets: Besides the exact compensation, the densities of both trap types, N_{tn} and N_{tp}, have to be at least $5 \times 10^{19}\ \mathrm{cm}^{-3}$ or higher, the energy level of the traps for the conduction controlling carrier (e.g., electrons, donor-like traps) has to be nominally 0.2 to 0.5 eV deeper in the gap than the carrier Imref (which is close to the electrode Fermi level at the interfaces), i.e., this traps are nominally slightly "deep," while the energy level of the compensating traps has to be shallow. Unfortunately, no significant feature was found in the simulation data why the described conditions result in nearly perfect PFE behavior and why this is changed by small excursions from the exact compensation, so that it may be possible that the perfect PFE slope was just hit by chance.

From all the data, it can be concluded that the appearance of PFE behavior in real measurements of current–field dependencies in thin film MIM stacks is rather improbable because of the unrealistic sharp condition of *exact* compensation at very high trap densities in a quite small range of examined parameter field. In addition, several other effects not yet implemented into the simulation tool (additional tunneling injection, asymmetric electrodes, severe change of trap potential barrier by potential overlap of neighboring traps at high trap densities) have been identified which may change the current–field dependence making the observation of PFE behavior even more improbable!

ACKNOWLEDGMENTS

This work was partially supported by the SFB 917 of the Deutsche Forschungsgemeinschaft (DFG), Germany.

[1]C. R. Crowell and S. M. Sze, Solid-State Electron. **9**, 1035 (1966).
[2]C. R. Crowell and M. Beguwala, Solid-State Electron. **14**, 1149 (1971).
[3]H. Schroeder, S. Schmitz, and P. Meuffels, Integr. Ferroelectr. **47**, 197 (2002).

[4]H. Schroeder, S. Schmitz, and P. Meuffels, Appl. Phys. Lett. **82**, 781 (2003).
[5]H. Schroeder and S. Schmitz, Appl. Phys. Lett. **83**, 4381 (2003).
[6]See www.webofknowledge.com for the keywords "Poole-Frenkel" AND "thin films".
[7]H. H. Poole, Philos. Mag. **32**, 112 (1916).
[8]J. Frenkel, Phys. Rev. **54**, 647 (1938).
[9]See, e.g., S. M. Sze, *Physics of Semiconductor Devices*, 2nd ed. (John Wiley & Sons, New York, USA, 1981), p. 402.
[10]K. C. Kao and H. Hwang, *Electrical Transport in Solids* (Pergamon Press Ltd., Oxford, UK, 1981), p. 148.
[11]H. Schroeder and S. Schmitz, in *Ferroelectric Thin Films XI* (Mater. Res. Soc. Symp. Proc. **748**, 423 (2003).
[12]See S. M. Sze, *Physics of Semiconductor Devices*, 2nd ed. (John Wiley & Sons, New York, USA, 1981), p. 259ff.
[13]F. Stöckmann, *Halbleiter-Probleme VI* (F. Vieweg, Braunschweig, Germany, 1961), p. 279.
[14]J. T. Li and X. L. Dong, Phys. Lett. A **340**, 303 (2005).
[15]J. D. Baniecki, R. B. Laibowitz, T. M. Shaw, C. Parks, J. Lian, H. Xu, and Q. Y. Ma, J. Appl. Phys. **89**, 2873 (2001).
[16]J. D. Baniecki, T. Shioga, K. Kurihara, and N. Kamehara, J. Appl. Phys. **94**, 6741 (2003).